Power Frequency Dependence of Space Charge Behavior and Partial Discharge Characteristics in SF_6 Gas

T. Takahashi, T. Yamada, N. Hayakawa and H. Okubo

Department of Electrical Engineering
Nagoya University, Japan

ABSTRACT

The partial discharge (PD) and breakdown (BD) characteristics in SF_6 gas under commercial and higher frequency (~600 Hz) ac voltage applications were investigated using high-speed electrical and optical measuring techniques with phase gate control method. Experimental results revealed that 400 Hz BD voltage at a certain gas pressure range was higher than that for 60 Hz and PD characteristics especially at the positive PD inception phase were much influenced by the applied power frequency. From these results, we clarified the dependence of space charge behavior on the applied power frequency and discussed the physical mechanism of PD and BD in SF_6 gas with consideration of the space charge behavior generated by PD in the previous half cycle of ac voltage.

1 INTRODUCTION

SF_6 gas has excellent properties for high voltage (HV) insulation and has been used widely for electric power apparatus like switchgear in gas-insulated system (GIS) and gas insulated transmission line (GIL) [1–3]. For the reliable operation of such apparatus, it is necessary to diagnose the insulation performance of the apparatus and thus the PD measurements are particularly important for the prediction of BD [4, 5].

Although many PD measuring methods have been proposed so far and used in practice [4, 6, 7], the fundamental mechanisms of PD generation in SF_6 gas have not yet been fully understood. This might be because the PD generation mechanism is so complicated that the predominant factors like space charge behavior are not quantitatively analyzed, so far. Therefore, it is essential to investigate the PD mechanism with consideration of the space charge behavior, particularly under ac voltage application in order to clarify the mechanism from PD inception to BD for the BD prediction technique [8]. Moreover, PD characteristics under ac voltage application at higher frequency than the commercial power frequency become more important for the discussion of GIS on-site testing with higher frequency applications [9, 10].

From the above viewpoints, in this paper we investigate the influence of the applied power frequency on PD and BD characteristics. We describe the measured results of phase-resolved PD generation characteristics, PD current pulses, and light emission characteristics using high-speed optical and electrical techniques. Based on these experimental results, we discuss the physical mechanism of PD and BD in SF_6 gas under ac voltage application with consideration of the space charge behavior.

2 EXPERIMENTAL

Figure 1 shows the experimental setup in this study. A high voltage (HV) source can provide ac voltage with frequency range from 60 to 600 Hz. To generate ac voltage with frequencies >60 Hz, a sinusoidal wave of a designated frequency was first generated by a signal generator. The sinusoidal wave signal was amplified to HV to 75 kV_{rms} by a power amplifier and a test transformer.

As a PD source, a stainless steel needle electrode was fixed on the HV conductor of a model GIS. The needle electrode had a length of 20 mm and hemispherical tip with a radius of 500 μm. A plane electrode with diameter of 30 mm was placed at 10 mm below the needle tip.

PD current pulses were measured by a high-speed digital oscilloscope (sampling rate: 5 GS/s, analog band width: 1 GHz) through the plane electrode and a matching circuit with wide frequency range; <1 MHz to >1 GHz [11]. The sensitivity of the PD current pulse height was <1 mA. Since the typical rise and fall times of the PD current pulse were ~1 ns, the sensitivity of the PD charge was calculated as 1 pC. On the other hand, a light emission image of PD was observed by a still

1070–9878/0/ $3.00 © 2000 IEEE

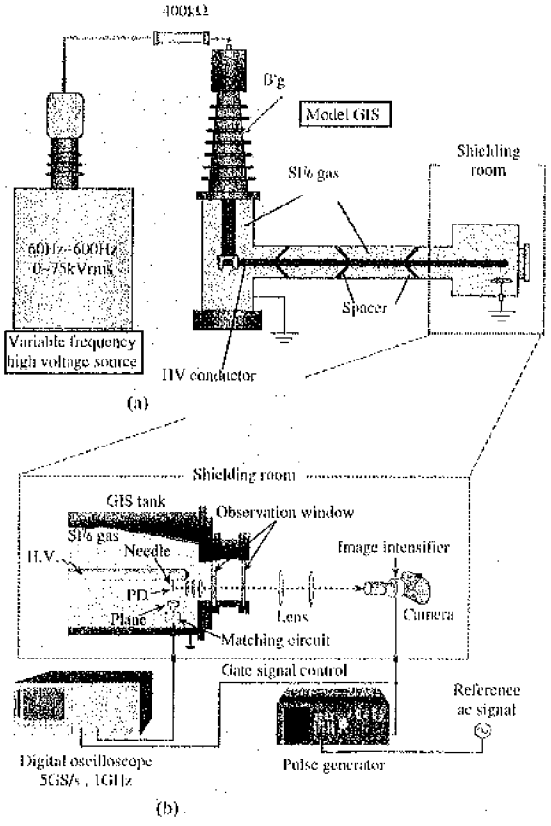

Figure 1. Experimental setup for measuring PD characteristics. (a) Model GIS and HV circuit. (b) Measurement system.

camera through an image intensifier (II). We already have developed a simultaneous measurement technique of PD current pulses and PD light emission images by using the 'phase gate control method' [12]. In that method, a gate signal with a designated pulse width, synchronized with the applied ac voltage phase, was generated by a pulse generator and put into the oscilloscope and the II. Thus, we can obtain the current pulse and the corresponding light image of a single PD during the designated phase width controlled by the gate signal.

The model GIS was filled with SF_6 gas and all experiments described in this paper were carried out at room temperature.

3 EXPERIMENTAL RESULTS

3.1 PD INCEPTION AND BREAKDOWN VOLTAGE

Figure 2 shows the positive and negative PD inception voltage (PDIV) ($PDIV_+$, $PDIV_-$), and the breakdown voltage (BDV) as a function of the gas pressure for the applied power frequencies $f = 60$ Hz and $f = 400$ Hz. As can be seen in Figure 2, $PDIV_-$ increases with the gas pressure and is independent of the power frequency. $PDIV_+$ also increases with the gas pressure; however, it clearly decreases with increasing power frequency from 60 to 400 Hz, and finally reaches the level of $PDIV_-$. On the other hand, BDV for $f = 60$ Hz once increases as the gas pressure P increases to P_m at which BDV reaches its maximum value, then decreases suddenly to the voltage level of $PDIV_+$ at the pressure P_c. At $P \geqslant P_c$, BDV increases again with the gas pressure. This nonlinearity of BDV curve also appears for $f = 400$ Hz. At $P \leqslant P_m$, BDV for $f = 400$ Hz has almost the same value as that for $f = 60$ Hz, while at $P \geqslant P_m$, it keeps a higher value than that for $f = 60$ Hz.

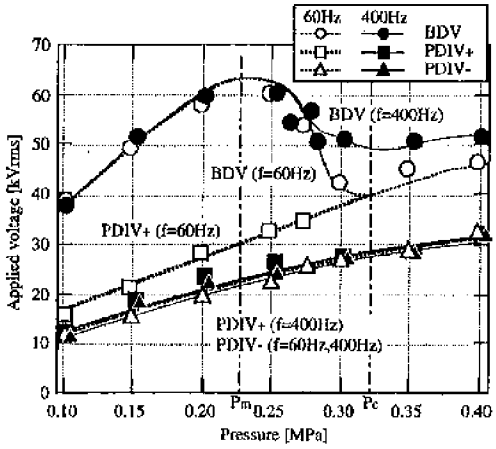

Figure 2. PDIV and BDV characteristics as a function of gas pressure for $f = 60$ Hz and $f = 400$ Hz ac voltage application. Needle electrode; $r = 500$ μm, $g = 10$ mm, in SF_6 gas.

$PDIV_+$, $PDIV_-$ and BDV as a function of the power frequency at $P = 0.1$ MPa are summarized in Figure 3. The decreasing dependence of $PDIV_+$ on the frequency is clearly shown.

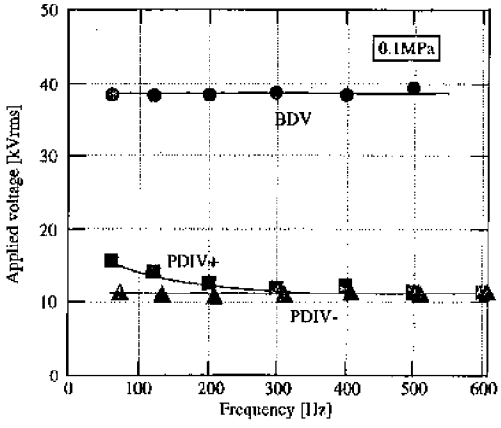

Figure 3. Power frequency dependence of positive and negative PD inception voltage ($PDIV_+$, $PDIV_-$) and BDV. Needle electrode; $r = 500$ μm, $g = 10$ mm, in SF_6 gas, $P = 0.1$ MPa.

In the following Sections, we will describe PD characteristics at $P \leqslant P_m$, especially at $P = 0.1$ MPa in order to compare the PD characteristics at the identical values of the applied ac voltage for different power frequencies. This is due to the similarities in BDV at $P \leqslant P_m$ as shown in Figure 2.

3.2 PD GENERATION CHARACTERISTICS

Figures 4(a) and (b) show the phase-resolved PD characteristics in SF_6 gas at $P = 0.1$ MPa and the applied voltage $V_a = 30\ kV_{rms}$, for

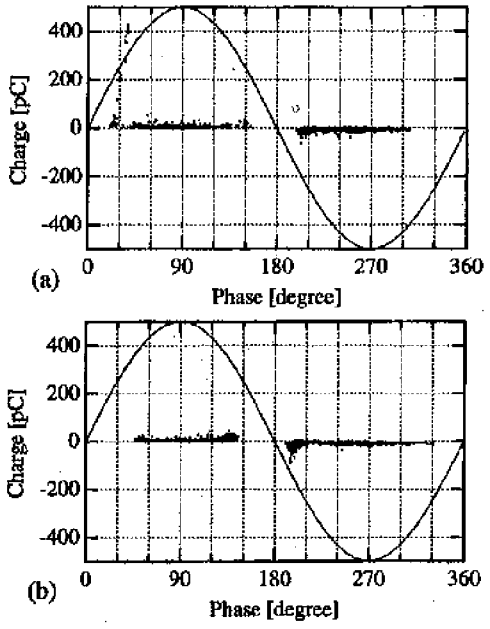

Figure 4. Phase-resolved PD characteristics. Needle electrode; $r = 500\ \mu$m, $g = 10$ mm, in SF_6 gas, $P = 0.1$ MPa, $V_a = 30\ kV_{rms}$, superimposed for 0.5 s. (a) $f = 60$ Hz, (b) $f = 400$ Hz.

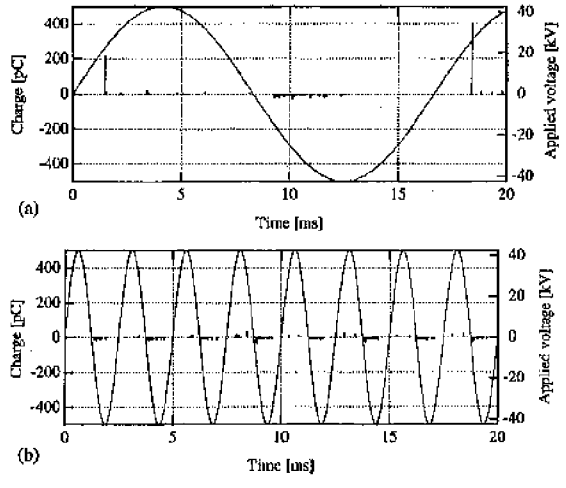

Figure 5. Time-resolved PD characteristics. Needle electrode; $r = 500\ \mu$m, $g = 10$ mm, in SF_6 gas, $P = 0.1$ MPa, $V_a = 30\ kV_{rms}$. (a) $f = 60$ Hz, (b) $f = 400$ Hz.

$f = 60$ Hz and $f = 400$ Hz, respectively. A single dot in the Figures shows an individual PD pulse. All of the PD during 0.5 s are plotted along with the PD generation phase. Figures 5(a) and (b) show the time-resolved PD characteristics under the same condition as Figures 4(a) and (b), respectively. As can be seen in Figure 4(a) for $f = 60$ Hz, positive PD, a relatively large charge magnitude occurs near the positive PD inception phase and is followed by PD having small charge magnitude. On the other hand, in Figure 4(b) for $f = 400$ Hz, only PD with small charge magnitude occur in the positive half cycle. PD in the negative half cycle, however, has relatively large charge magnitude at near negative PD inception phase for both $f = 60$ Hz and $f = 400$ Hz. Note that the maximum charge magnitude for $f = 400$ Hz is larger than that for $f = 60$ Hz, which is in inverse proportion to the positive PD characteristics.

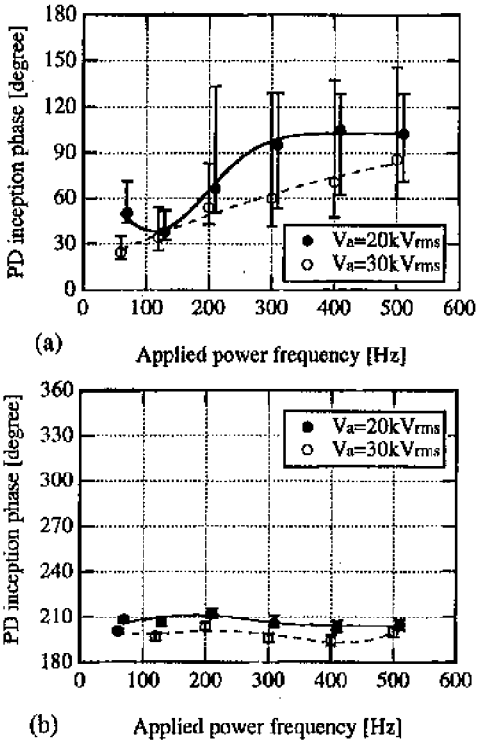

Figure 6. Power frequency dependence of PD inception phase. Needle Electrode; $r = 500\ \mu$m, $g = 10$ mm, in SF_6 gas, $P = 0.1$ MPa. (a) Positive PD, (b) negative PD.

These characteristics can be seen more clearly in Figures 5(a) and (b). PD with relatively large charge magnitude occurs first and is followed by PD with small charge magnitude in the positive half cycle for $f = 60$ Hz. On the other hand, only PD with small charge magnitude occurs in the positive half cycle for $f = 400$ Hz.

3.3 INSTANTANEOUS VOLTAGE AT PD INCEPTION PHASE

In this Section, we define the voltage phase at which a positive PD pulse first was observed in each positive half cycle of applied ac voltage as the positive PD inception phase, and also that in negative half cycle as the negative PD inception phase. Figures 6(a) and (b) show the applied power frequency dependence of the PD inception phase in each cycle of the applied ac voltage for positive and negative PD, respectively. In Figures 6(a) and (b), the solid line shows the measurement results at $V_a = 20\ kV_{rms}$,the broken line shows those at $V_a = 30\ kV_{rms}$. The experiments were iterated at least 10 times to plot data under each set of conditions. As shown in Figure 6(a), positive PD inception phase at $V_a = 20\ kV_{rms}$ for $f = 60$ Hz is ~50° to ~70° and tends to increase with the power frequency. Finally, PD tends to start in the phase region of the positive applied voltage peak. This phase shift for positive PD

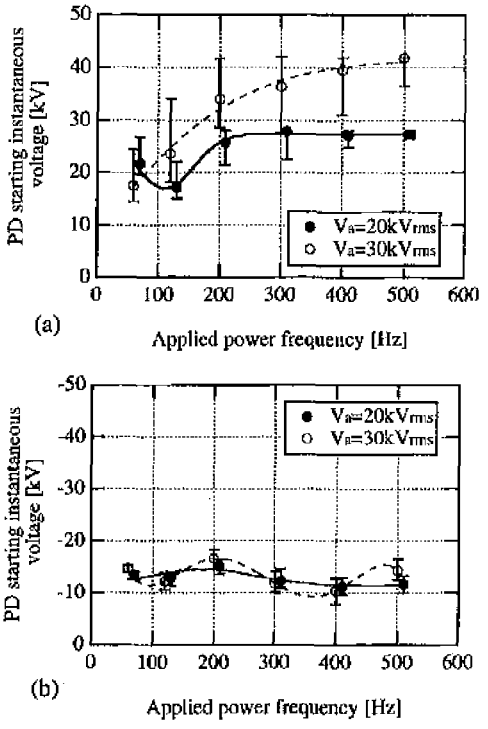

Figure 7. Power frequency dependence of PD starting instantaneous voltage. Needle Electrode; $r = 500\ \mu$m, $g = 10$ mm, in SF_6 gas, $P = 0.1$ MPa. (a) Positive PD, (b) negative PD.

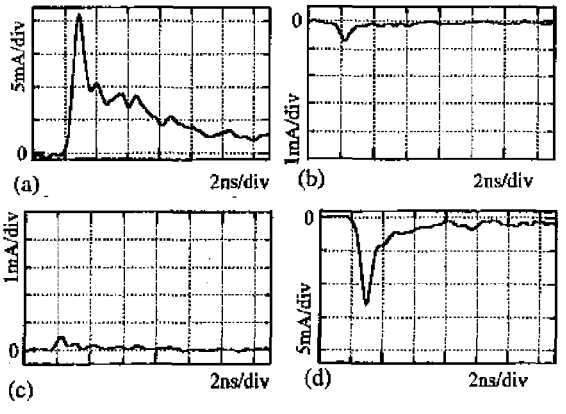

Figure 8. Typical PD current pulse waveforms. Needle Electrode; $r = 500\ \mu$m, $g = 10$ mm, in SF_6 gas, $P = 0.1$ MPa, $V_a = 30\ kV_{rms}$. (a) $f = 60$ Hz, $\phi = 30°$, (b) $f = 60$ Hz, $\phi = 200°$, (c) $f = 400$ Hz, $\phi = 40°$, (d) $f = 400$ Hz, $\phi = 200°$.

inception can also be seen at $V_a = 30\ kV_{rms}$. On the other hand, in Figure 6(b), negative PD inception phases at both $V_a = 20\ kV_{rms}$ and $V_a = 30\ kV_{rms}$ are almost independent of the power frequency and hold ~205° for $V_a = 20\ kV_{rms}$ and ~195° for $V_a = 20\ kV_{rms}$.

Next, the power frequency dependence of the instantaneous voltage at positive and negative PD inception phases are shown in Figures 7(a) and (b), respectively. As can be seen in Figure 7(a), positive PD at both $V_a = 20\ kV_{rms}$ and $V_a = 30\ kV_{rms}$ starts near the instantaneous voltage $V_{inst} = 20$ kV for $f = 60$ Hz. The instantaneous voltage at

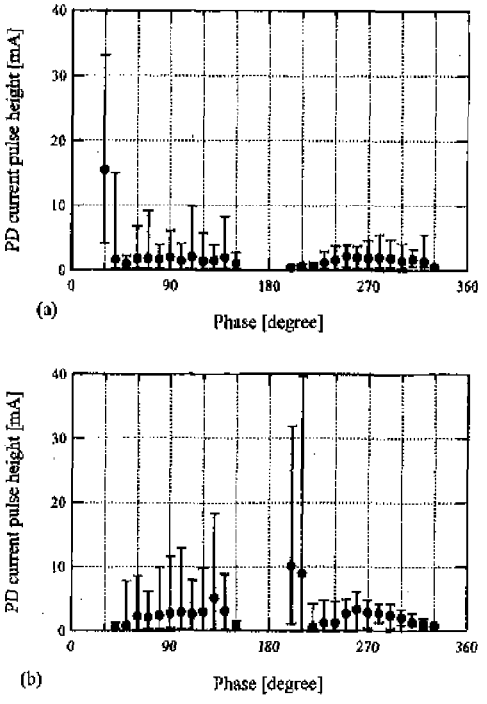

Figure 9. Phase dependence of PD current pulse height. Needle Electrode; $r = 500\ \mu$m, $g = 10$ mm, in SF_6 gas, $P = 0.1$ MPa, $V_a = 30\ kV_{rms}$. (a) $f = 60$ Hz, (b) $f = 400$ Hz.

positive PD inception tends to increase with the frequency, and then the positive PD for $f = 400$ to 500 Hz starts near the peak value of the applied voltage; $V_{inst} = 28$ kV for $V_a = 20\ kV_{rms}$ and $V_{inst} = 40$ to 42 kV for $V_a = 30\ kV_{rms}$, respectively. On the contrary, the instantaneous voltage at negative PD inception phase shown in Figure 7(b) is almost independent of the applied voltage and frequency.

3.4 PD CURRENT PULSE WAVEFORM

Figures 8(a) to (d) show typical PD current pulse waveforms observed at 30° and 200° for $f = 60$ Hz, at 40° and 200° for $f = 400$ Hz, respectively, in the vicinities of the positive and negative PD inception phases for both applied power frequencies. As seen in Figure 8, not only the pulse height but also the waveform of the PD current pulses are quite different at each frequency. In positive PD, the pulse height for $f = 60$ Hz in Figure 8(a) is larger than that for $f = 400$ Hz in Figure 8(c). In negative PD, the pulse height for $f = 60$ Hz in Figure 8(b) is smaller than that for $f = 400$ Hz in Figure 8(d).

Similar experiments were carried out for different phase regions. We divided a single ac cycle into 36 regions (every 10°) and measured the current pulse waveforms 30 times for each phase region. Figures 9(a) and (b) show the obtained phase dependence of the PD current pulse height for $f = 60$ Hz and $f = 400$ Hz, respectively. Note that each PD current pulse waveform achieved in the measurement had a pulse-like waveform with a steep wave front. As seen in Figures 9(a) and (b), the PD pulse height characteristics for $f = 60$ Hz shows a similarity to that for $f = 400$ Hz except in the positive and negative PD inception

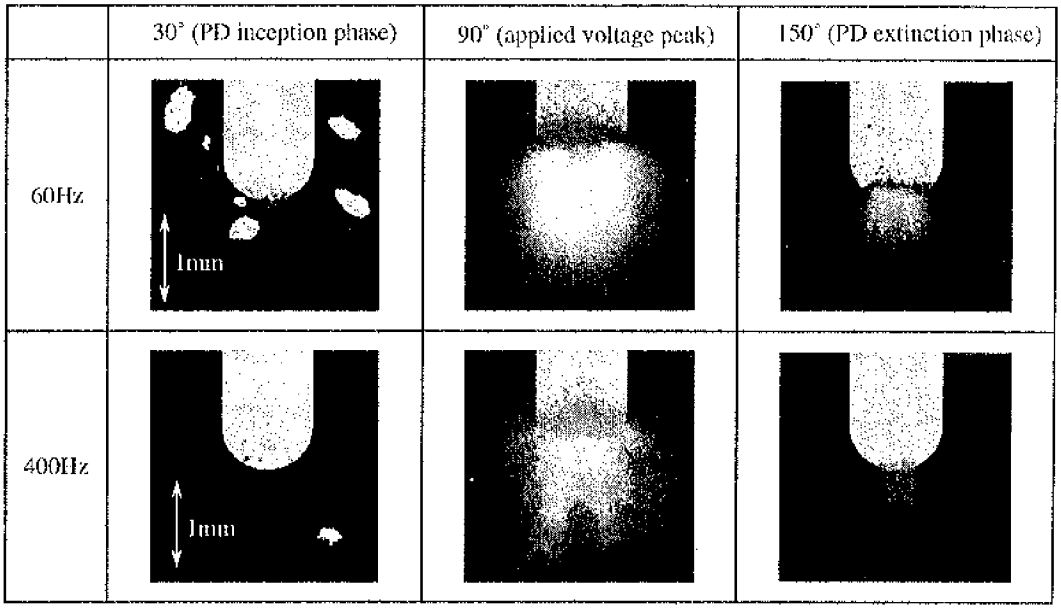

Figure 10. Light emission images of positive PD at the tip of a needle electrode for different power frequencies and phases. Needle electrode; $r = 500\ \mu$m, $g = 10$ mm, in SF_6 gas, $P = 0.1$ MPa, $V_a = 30\ kV_{rms}$, Gate width: 10° (463.0 μs for $f = 60$ Hz, 69.44 μs for $f = 400$ Hz), superimposed for 60 ac cycles.

phases. For $f = 60$ Hz, PD with large pulse height occurs near the positive PD inception phase, followed by PD with small pulse height, while for $f = 400$ Hz, the PD pulse height is kept small, even near the positive PD inception phase. Near the negative PD inception phase, PD with relatively large pulse height occurs, with magnitude larger for $f = 400$ Hz than for $f = 60$ Hz.

3.5 POSITIVE PD LIGHT EMISSION IMAGES

Figure 10 shows the light emission images of positive PD at $V_a = 30\ kV_{rms}$ for $f = 60$ Hz and $f = 400$ Hz, at 30°, 90° and 150°, respectively. Note that the light emission in each image was superimposed within the gate width of 10° (463.0 μs for $f = 60$ Hz, 69.44 μs for $f = 400$ Hz) near the designated phase for 60 cycles of the applied ac voltage. As seen in Figure 10, PD occurring at 90° and 150° show brush-like luminous images for both $f = 60$ Hz and $f = 400$ Hz. Here, the 'streamer type' PD generally spreads out around the needle tip, which is assumed to look like a brush if the repetition rate is higher, and has a current pulse with steep wave front [13]. Thus, PD at 90° and 150° for both $f = 60$ Hz and $f = 400$ Hz can be recognized as the 'streamer type' PD, from viewpoints of both the light emission of brush-like image in Figure 10 and the current pulse with steep wave front in Figure 9.

On the other hand, PD occurring at 30° for $f = 60$ Hz and $f = 400$ Hz are dot-like images. PD at 30° for $f = 60$ Hz spreads out around the needle tip and has a pulse-like current waveform with large amplitude as shown in Figure 8(a). Thus, PD at 30° for $f = 60$ Hz is also the 'streamer type' PD with small repetition rate. On the contrary, PD at 30° for $f = 400$ Hz spreads over the needle tip surface, which looks like a thin film, and pulse-like current waveform has never been observed as shown in Figure 9 (b). Therefore, PD at 30° for $f = 400$ Hz might be a 'glow' discharge which is characterized by the non-pulsive current waveform and the luminous image covering the needle tip [13].

4 DISCUSSION

4.1 PD INCEPTION VOLTAGE AND ION DRIFT SIMULATION

4.1.1 PD INCEPTION VOLTAGE

In general, positive PD is generated by an electron initiated by collision detachment of negative ions in the high electric field region [8]. Thus, positive PD generation depends on whether or not negative ions exist around the needle tip. Under ac voltage application, the negative ions at positive PD inception phase can be derived from PD in the previous negative half cycle and/or cosmic rays. In the case of needle-plane electrode geometry, the high field region initiating PD is so restricted that, even under continuous ac voltage application, the generation of an initial electron would be the necessary condition for PD initiation. On the other hand, negative PD is generated by an initial electron derived from the field emission from the electrode surface. Thus, the generation of an initial electron for negative PD depends only on the electric field strength on the electrode surface. Therefore, an initial electron can be generated more easily for negative PD than for positive PD, and the resultant $PDIV_-$ is equal to or smaller than $PDIV_+$.

For the low power frequency $f = 60$ Hz, at $PDIV_-$, the negative ions generated by PD in the negative half cycle may be swept away until the applied voltage polarity was reversed from negative to positive. This is due to the drift and diffusion of the negative ions toward the plane electrode and the neutralization at the electrode surface. As the applied voltage increases, the existing probability of residual negative ions near

the needle tip is increased, and the resultant generation probability of initial electrons for positive PD inception in the subsequent positive half cycle, also is increased. Therefore, $PDIV_+$ becomes higher than $PDIV_-$ for $f = 60$ Hz as shown in Figures 2 and 3.

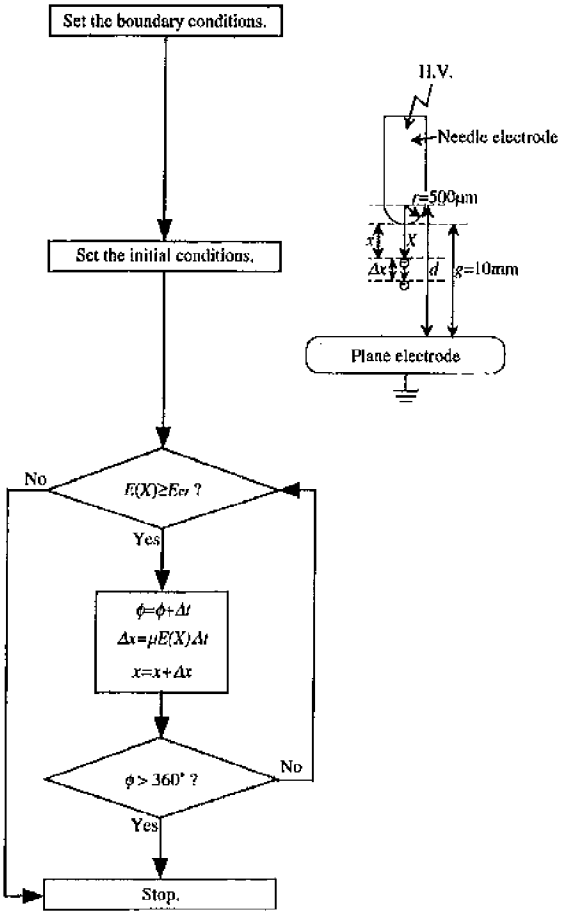

Figure 11. Flow chart of the calculation of ion drift. Ion mobility $\mu = 0.65\times10^{-4}$ [(m/s)/(V/m)], tip radius $r = 500\times10^{-6}$ [m], gap length $g = 10\times10^{-3}$ [m], gas pressure $P = 0.1\times10^{6}$ [Pa], critical electric field $E_o/P = 89$ [V/m/Pa], charge: negative ion, applied frequency $f = 60$ Hz or 400 Hz, applied voltage $V_a = 12.7\times10^{3}$ [V_{rms}], phase step: $\Delta\phi = 0.001$ [°], time step: $\Delta t = 46.3\times10^{-9}$ [s] ($f = 60$ Hz), 6.94×10^{-9} [s] ($f = 400$ Hz). ϕ: applied voltage phase [°], ϕ_0: initial phase, $\phi_0 = 270°$, x: distance between needle tip and the ion [m], x_0: initial position of the ion, $x_0 = 0.3\times10^{-3}$ [m], Electric field strength: $E(X) = (2rd)/(2d-r)\{1/X^2 - 1/(2d-X)^2\}V_{inst}$ [V/m], $X = r + x$, $d = g + r$, $V_{inst} = \sqrt{2}V_a \sin(2\pi\phi/360)$

On the other hand, for the higher frequency at $f = 400$ Hz, most negative ions generated by PD in the negative half cycle can remain at the polarity reversal. Thus, enough initial electrons exist to generate positive PD in the subsequent positive half cycle. Therefore, $PDIV_+$ for the higher frequency is reduced and finally becomes equal to $PDIV_-$.

4.1.2 ION DRIFT SIMULATION

In order to quantitatively verify the existence of the larger residual ions in the gap space at higher frequency, we calculated the negative ion drift from the negative PD generation phase (270°) to the polarity reversal (360°) in every 0.001° phase step. Figure 11 shows the flow chart of the calculation. We calculated the static electric field with the electric image method under the ion mobility $\mu = 0.65\times10^{-4}$ [(m/s)/(V/m)] [14] for a negative ion such as SF_6^-. The collision between the ion and other particles as well as the electric field formed by the space charges were neglected. Initially the ion was assumed to be located at 0.3 mm below the needle tip, where the extension length of negative PD was maximum. The applied voltage was set at 12.7 kV_{rms}, which is just above $PDIV_-$ for both $f = 60$ Hz and $f = 400$ Hz.

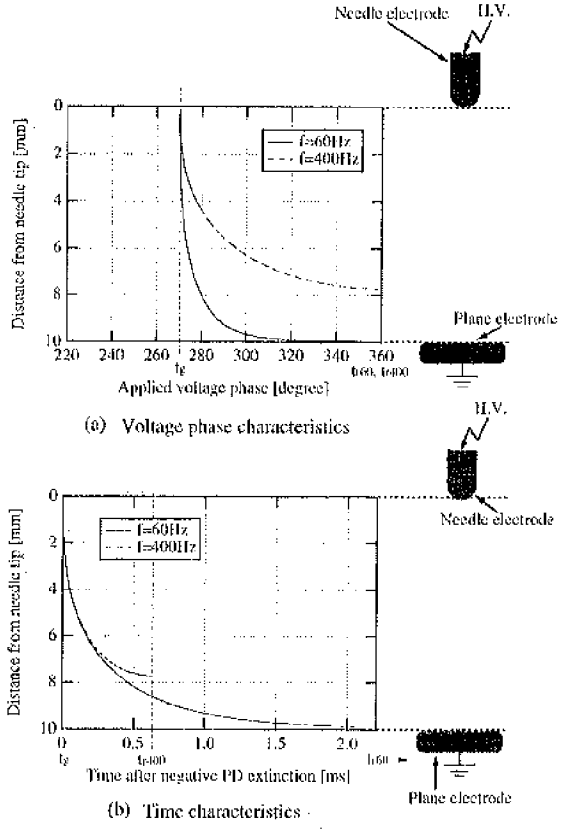

Figure 12. Calculation of the path of the negative ion drift. Needle Electrode; $r = 500$ μm, $g = 10$ mm, in SF_6 gas, $P = 0.1$ MPa, $V_a = 12.7$ kV_{rms}. (a) Voltage phase characteristics, (b) time characteristics.

Figure 12 shows the path of the negative ion drift along the gap axis calculated for $f = 60$ Hz and $f = 400$ Hz as functions of (a) voltage phase and (b) time after the ion generation. In Figure 12, we defined the time when the negative PD was generated (270°) as t_g and the time when the applied voltage polarity was reversed from negative to positive for $f = 60$ Hz and $f = 400$ Hz as t_{r60} and t_{r400}, respectively. As can be seen in Figure 12, the negative ion for $f = 60$ Hz reaches the plane electrode at the polarity reversal t_{r60}. On the contrary, for $f = 400$ Hz, the negative ion drifts 7.7 mm below the needle tip at the polarity reversal t_{r400}, and does not reach the plane electrode. This simulation result suggests that the amount of the residual negative ions at the polarity reversal for $f = 400$ Hz is much larger than that for $f = 60$ Hz at $PDIV_-$. Thus, a larger number of residual negative ions

[9] W. Hauschild, J. Spiegelberg and E. Lemke, "Frequency-Tuned Resonant Test Systems for HV On-site Testing of SF_6-Insulated Apparatus", Proceedings of the 10th International Symposium on HV Engineering, Vol. 4, pp. 457–460, 1997.

[10] J. Gorablenkow, T. Huecker and U. Schichler, "Application of UHF Partial Discharge Monitoring and Expert System Diagnosis", Conference Record of the 1998 IEEE International Symposium on Electrical Insulation, Vol. 1, pp. 61–64, 1998.

[11] H. Okubo, A. Suzuki, T. Kato, N. Hayakawa and M. Hikita, "Frequency Component of Current Pulse Waveform in Partial Discharge Measurement", Proceedings of the 9th International Symposium on HV Engineering, No. 5634, 1995.

[12] H. Okubo, M. Yoshida, T. Takahashi, M. Hikita, H. Watanabe and N. Hashimoto, "Investigation of Partial Discharge Mechanism in SF_6 Gas by Simultaneous Measurement of Current Waveform and Light Emission", Proceedings of the 10th International Symposium on HV Engineering, Vol. 2, pp. 177–180, 1997.

[13] O. Farish, O. E. Ibrahim and A. Kurimoto, "Prebreakdown Corona Processes in SF_6 and SF_6/N_2 Mixtures", Proceedings of the 3rd International Symposium on HV Engineering, No. 31. 15, 1979.

[14] J. de Urquijo-Carmona, I. Alvarez, H. Martinez and C. Cisneros, "Mobility and Longitudinal Diffusion of SF_5^- and SF_6^- in SF_6", Journal of Physics D: Applied Physics, Vol. 24, No. 5, pp. 664–667, 1991.

[15] G. W. Trichel, "The Mechanism of the Negative Point to Plane Corona Near Onset", Physical Review, Vol. 54, pp. 1078–1084, 1938.

[16] A. V. Phelps and R. J. Van Brunt, "Electron-transport, Ionization, Attachment, and Dissociation Coefficients in SF_6 and its Mixtures", Journal of Applied Physics, Vol. 64, pp. 4269–4277, 1988.

[17] F. Pinnekamp and L. Niemeyer, "Qualitative Model of Breakdown in SF_6 in Inhomogeneous Gaps", Journal of Physics D: Applied Physics, Vol. 16, pp. 1293–1312, 1983.

Manuscript was received on 7 January 1999, in final form 21 August 1999.